UVicSPACE: Research & Learning Repository

University of Victoria

Faculty of Science

Faculty Publications

This is a post-review version of the following article:

Validation of Inner, Second, and Outer Sphere Contributions to T_1 and T_2 Relaxation in Gd^{3+}-Based Nanoparticles Using Eu^{3+} Lifetime Decay as a Probe

Armita Dash, Barbara Blasiak, Boguslaw Tomanek and Frank C.J.M. van Veggel

May 2018 (online)

The final publication will be available at:

http://dx.doi.org/10.1021/acs.jpcc.8b02807

Citation for this paper:

Dash, A., Blasiak, B., Tomanek & van Veggel, F.C.J.M. (2018). Validation of Inner, Second, and Outer Sphere Contributions to T_1 and T_2 Relaxation in Gd^{3+}-Based Nanoparticles Using Eu^{3+} Lifetime Decay as a Probe. *The Journal of Physical Chemistry C*, 122(21), 11557-11569. http://dx.doi.org/10.1021/acs.jpcc.8b02807

Validation of Inner, Second, and Outer Sphere Contributions to T_1 and T_2 Relaxation in Gd^{3+}-based Nanoparticles using Eu^{3+} Lifetime Decay as a Probe

Armita Dash,[†‡] *Barbara Blasiak,*[§⊥] *Boguslaw Tomanek*[§⊥‖] *and Frank C. J. M. van Veggel*[†‡]*

[†]Department of Chemistry, University of Victoria, Victoria, British Columbia V8W 2Y2, Canada

[‡]The Centre for Advanced Materials and Related Technology, University of Victoria, Victoria, British Columbia V8W 2Y2, Canada

[§]Experimental Imaging Centre, University of Calgary, Calgary, Alberta T2N 4N1, Canada

[⊥]Institute of Nuclear Physics, Polish Academy of Sciences, 31-342 Krakow, Poland

[‖]Department of Oncology, Faculty of Medicine & Dentistry, University of Alberta, Edmonton, Alberta T6G 2T4, Canada

ABSTRACT

Paramagnetic lanthanide-based NPs are currently designed as magnetic resonance imaging (MRI) contrast agents to obtain optimal relaxivities at high magnetic fields of 7, 9.4 and 11.7 T where human imaging has been possible yielding high contrast to noise ratio in the MR images compared to the clinical field of 3 T. However, the underlying longitudinal (T_1) and transverse (T_2) relaxation mechanisms of the NP-based contrast agents based on the spatial motion and proximity of water protons with respect to the paramagnetic ions on the surface of NPs are still not well understood, specifically, in terms of contributions from inner, second, and outer spheres of coordination of water molecules to the NPs. Gd^{3+}-based NPs, e.g., $NaGdF_4$, are promising T_1 contrast agents owing to the paramagnetic Gd^{3+} possessing a symmetric $^8S_{7/2}$-state and slow electronic relaxation relevant to its efficiency to produce a positive (T_1) contrast. Here, water-dispersed $NaGdF_4:Eu^{3+}$ (3 nm diameter, TEM) and $NaYF_4$-$NaGdF_4:Eu^{3+}$ core-shell NPs (18.3 nm core diameter with 0.5 nm thick shell, TEM) were studied for their r_1 and r_2 relaxivities at 9.4 T. Excited state lifetime decays of Eu^{3+} dopants, which are highly sensitive to proximate water molecules, were analyzed, demonstrating a dominance of inner and second sphere contribution over outer sphere to the T_1 and T_2 relaxations in smaller $NaGdF_4:Eu^{3+}$ NPs while exclusively outer sphere in $NaYF_4$-$NaGdF_4:Eu^{3+}$ core-shell NPs.

INTRODUCTION

Magnetic resonance imaging (MRI) is a non-invasive diagnostic technique that produces tomographic information about whole tissue samples, animals and humans with high spatial resolution and excellent soft tissue contrast.[1] The radiofrequency (RF) pulses, external static magnetic field and time variable magnetic fields influence the nuclear spin of water protons allowing MR signal acquisition and image reconstruction. Following RF excitation longitudinal or spin-lattice (T_1) and transverse or spin-spin (T_2) relaxation processes at the tissue sites generate contrast in the MR image. Contrast agents are often introduced to enhance the relaxation rates of water protons and, thus, improve diagnostic capabilities of MRI.[2-6] Such agents, in the form of chelates of paramagnetic lanthanide (Ln^{3+}) ions, for example, Gd^{3+} possessing half-filled *f*-orbitals with 7 unpaired electrons, have widely been studied and employed clinically due to their ability to effectively shorten the T_1 proton relaxation time.[7] Despite progress in their design and synthesis, Gd^{3+} chelates are limited by low specificity, short blood half-life, fast renal clearance and very low relaxivity at high magnetic fields ($\geq$ 3 T).[2-4,7-8] To overcome these constraints, nanoparticle (NP) based contrast agents, possessing high density of metal ions per NP probe, are being developed and can be used at low doses or detect low concentration targets, thereby, mitigating dosage toxicity issues.[9-12] Their physiochemical, surface and magnetic properties can be tuned to generate MR images with high contrast-to-noise ratio at high magnetic fields. A high magnetic field, such as 9.4 T, is advantageous over low fields (< 3 T) because it yields images with high signal to noise ratio, hence high spatial resolution and/or reduced acquisition time. These benefits have led to the need for human imaging at 7, 9.4 and even 11.7 T.[13-16] To design and optimize potential NP-based contrast agents for MRI applications, it is essential to understand the mechanism of how the NPs influence the relaxation rates (relaxivities) of surrounding water protons to produce the image contrast.

An NP, containing paramagnetic Ln^{3+} ions (e.g., Gd^{3+}) and dispersed in water, can be viewed as having three consecutive solvation spheres: (i) the inner sphere (IS) where the ligands/water molecules directly coordinate to surface Gd^{3+} ions and follow the NPs in its Brownian reorientation and exchange with the surrounding free water molecules, (ii) the second sphere (2S) where the water molecules significantly bind to the surface coating ligands of the NP, develop an electrostatic interaction with the surface lanthanide and sodium cations of the

NP, rotate with the NP and exchange with the surrounding free water molecules and the ones coordinated to the ligands, and (iii) the outer sphere (OS) where free water molecules translate, diffuse, and rotate with their Brownian motion with respect to the NP.[2,17-18] Relaxivity of NPs is influenced by the proximity of water protons to the Gd^{3+} ions. The penetration of water in any of the solvation spheres is entirely governed by the surface functionalization of the NP. Although several theoretical studies and nuclear magnetic relaxation dispersion profiling have been carried out to understand the parameters regulating the relaxation rates of Gd^{3+} ions when water diffuses into the inner, second, or/and outer spheres of coordination,[2,7,19-20] there is no direct experimental evidence that elucidates the proportion of contribution of inner, second, or/and outer sphere relaxation mechanisms towards the relaxivities of Ln^{3+}-based NPs. Articles simply assume one or the other for the interpretation of the results.

In this work, we investigate the water permeation into the solvation spheres of PVP (polyvinylpyrrolidone) and DSPE-mPEG [1,2-distearoyl-*sn*-glycero-3-phosphoethanolamine-*N*-{methoxy(polyethylene glycol)}] coated $NaGdF_4:Eu^{3+}$ NPs (3 nm core diameter) and $NaYF_4$-$NaGdF_4:Eu^{3+}$ core-shell NPs (18.3 nm core diameter with a shell thickness of 0.5 nm) by analyzing the excited state lifetime decay of trivalent europium Eu^{3+} ions doped in these NPs to understand the contribution of inner, second, and/or outer sphere relaxation mechanisms towards the relaxivities of NPs at 9.4 T. Eu^{3+} is well known for its strong luminescence in the red spectral region due to its characteristic emission transitions from the $^5D_0$ to the ^7F_J manifolds (J = 0–6).[21-22] Eu^{3+} doped in a low phonon energy (~360 cm^{-1}) bearing fluoride host has widely been studied for optical and optoelectronic applications.[23] Also, Eu^{3+} ions at the ground state are not expected to influence the paramagnetic properties of the NPs because the total electronic angular momentum of Eu^{3+}, J, is zero (Eu^{3+}, $4f^6$, $L = S = 3$).[24] The surface features of particles of nanosize dimensions play a vital role in influencing the luminescence properties of Eu^{3+} due to the particle's large surface to volume ratio.[25] Furthermore, the photoluminescence intensity of Eu^{3+} is sensitive to O–H vibrations in proximate water molecules, thus, yielding an excellent tool to probe water accessibility to Eu^{3+} ions on the surface of the NPs. As such, emission and excited state decay times of Eu^{3+} were investigated in two differently sized Gd^{3+}-based NPs serving as potential T_1-contrast agents: (1) $NaGdF_4$ NPs doped with Eu^{3+} (3 nm core diameter) and (2) $NaYF_4$-$NaGdF_4$ core-shell NPs (18.3 nm $NaYF_4$ core diameter) with a 0.5 nm thick $NaGdF_4$ shell doped with Eu^{3+}. Both types of NPs were synthesized in an organic medium containing

oleic acid and octadecene. These NPs dispersed in hexanes are then coated with PVP or DSPE-mPEG, which are water soluble molecules that impart excellent biocompatibility and hydrophilicity to the NPs.[26-27] The smaller NPs have a mean curvature of about 6 times larger than the bigger core-shell NPs which may provide easy accessibility of water molecules to coordinate to the surface cations of smaller NPs. In case of PVP coated NPs, the oleate ligands on the surface of the NPs are completely replaced by the PVP molecules,[26] this may allow water access to the surface cationic sites of NPs. On the other hand, in DSPE-mPEG coated NPs, the oleate ligands remain on the NP surface as their alkyl chains interlock with the distearoyl phosphoethanolamine moieties of DSPE-mPEGs via hydrophobic interactions and the PEGs interact with the aqueous environment, likely allowing no direct access of water molecules to the surface of the NPs. The surface coatings of PVP and DSPE-mPEG were assessed with the extent of water accessibility by analyzing the lifetime decay curves of Eu^{3+}. MR relaxivity measurements were performed for PVP and DSPE-mPEG coated $NaGdF_4$ NPs at 9.4 T to correlate the underlying relaxation mechanism with the lifetime curves.

The excited state lifetime decay of Eu^{3+} ions which are present on the surface of NPs and are in proximity of water molecules prove to be an ideal probe to investigate the contribution of inner, second, and outer sphere relaxivities in NPs, thus, providing an appropriate approach to design NP-based MRI contrast agents.

EXPERIMENTAL SECTION

Chemicals. Gadolinium(III) oxide (99.9%), gadolinium(III) chloride hexahydrate (99.9%), europium(III) oxide (99.9%), europium(III) chloride hexahydrate (99.9%), yttrium(III) acetate hydrate, sodium trifluoroacetate (98%), ammonium fluoride (≥ 99.99%), polyvinylpyrrolidone (PVP-10, MW 10,000 Da), oleic acid (tech grade, 90%), 1-octadecene (tech grade, 90%), deuterium oxide (99.9%) and hexanes were purchased from Sigma Aldrich. Oleylamine (97%) was purchased from Acros, dichloromethane (DCM) from EMD chemicals, sodium hydroxide, trifluoroacetic acid, dimethyl sulphoxide (99.9%), toluene, dimethylformamide (DMF), anhydrous ethanol and methanol from Caledon laboratories and 1,2-distearoyl-*sn*-glycero-3-

phosphoethanolamine-*N*-[methoxy(polyethylene glycol)-2000] (ammonium salt) from Avanti Polar Lipids.

Synthesis of hexagonal (*β*) phase $NaGdF_4$ NPs.[11] $GdCl_3.6H_2O$ (1 mmol), oleic acid (4 mL) and 1-octadecene (15 mL) were stirred together in a 100 mL three-necked round bottom flask and heated at 140 ^oC under vacuum until a clear solution formed. It was cooled down to room temperature after which a solution of NaOH (2.5 mmol) and NH_4F (4 mmol) in methanol (10 mL) was added. The reaction mixture was stirred at room temperature for 1 h. It was heated to 80 ^oC to remove methanol under an argon flow. Subsequently, the solution was heated (15 ^oC/min) and maintained at 260 ^oC for 10 min under an argon flow. It was cooled to room temperature under air and the NPs were precipitated using 60 mL of ethanol, centrifuged (7,000 *g*, 10 min, Beckman Coulter Spinchron 15-rotor F0830) and washed with 60 mL of ethanol thrice. The collected NPs were dispersed in 10 mL of hexanes. To synthesize 5% Eu^{3+}-doped *β*-$NaGdF_4$ NPs, $GdCl_3.6H_2O$ (0.95 mmol) and $EuCl_3.6H_2O$ (0.05 mmol) were used in this procedure.

Synthesis of 5% Eu^{3+}-doped cubic (*α*) phase $NaGdF_4$ NPs (denoted as $NaGdF_4$:Eu^{3+} NPs). Gd_2O_3 (0.95 mmol), Eu_2O_3 (0.05 mmol) and 50% trifluoroacetic acid (10 mL) were mixed together in a 100 mL three-necked round bottom flask and refluxed at 85 °C for 5 h. Excess water was evaporated at 65 °C overnight to yield gadolinium trifluoroacetate. Sodium trifluoroacetate (2 mmol), oleic acid (5 mL), oleylamine (5 mL) and 1-octadecene (10 mL) were added to it and heated at 130 °C for 45 min under vacuum to remove residual water and oxygen. Subsequently, the solution was heated to 285 °C under an argon atmosphere and stirred vigorously for 45 min. The solution was cooled down to room temperature in air. The NPs were precipitated and washed with 60 mL of ethanol thrice by centrifugation (7,000 *g*, 10 min, Beckman Coulter Spinchron 15-rotor F0830) and finally dispersed in 10 mL of hexanes.

Synthesis of hexagonal (*β*) phase $NaYF_4$-$NaGdF_4$ core-shell NPs with the shell doped with 5% Eu^{3+} (denoted as $NaYF_4$-$NaGdF_4$:Eu^{3+} core-shell NPs).[28] Yttrium (III) acetate hydrate (1 mmol), oleic acid (6 mL) and 1-octadecene (17 mL) were mixed in a 100 mL three-necked round bottom flask and stirred under vacuum at 130 °C for 45 min. The solution was cooled to room temperature, added with a solution of NaOH (2.5 mmol) and NH_4F (4 mmol) in methanol (10 mL) and stirred for 1 h. Methanol was removed thereafter at 80 °C. The temperature was raised

to 300 °C (15 °C/min) under argon flow and the solution was stirred vigorously for 1 h. The cubic (α) $NaGdF_4$ (Eu^{3+}-doped) NPs in 1-octadecene (1 mL) was injected into the solution and stirred at 300 °C for 10 min to form a core-shell nanocrystal structure. The solution was cooled down to room temperature under air condition. The NPs were precipitated and washed with 60 mL of ethanol thrice by centrifugation (7,000 *g*, 10 min, Beckman Coulter Spinchron 15-rotor F0830) and finally dispersed in 10 mL of hexanes.

Phase transfer of NPs to water (and/or D_2O) using PVP-10.[11] Oleate capped NPs were exchanged with PVP-10 (molecular weight of 10,000 Da) in 1:1 DCM and DMF solvent mixture, refluxed at 85 ^oC for 18 h. NPs were precipitated in ethyl ether (100 mL) and dried under vacuum for 15 min. The amount of polymer for exchange was based on the NP size and calculated as such to accommodate ~60 PVP molecules per nm^2 of NP surface. After the exchange NPs were dispersed in appropriate solvents (deionized water and/or D_2O).

Phase transfer of NPs to water using phospholipids.[27] NPs were dispersed in 0.4 mL toluene at 7.0 mg/mL and added with DSPE-mPEG in 0.8 mL chloroform taking appropriate weight ratio of DSPE-mPEG to NP. 4 mL of DMSO was added slowly to the solution which was then incubated on a shaker for 30 minutes at room temperature. Chloroform and toluene were removed completely by vaporization under vacuum. Deionized water was added to the colloidal solution in DMSO to reach a total volume of 20 ml. DMSO was completely substituted with deionized water by three rounds of centrifugation in centrifugal filter tubes (Vivaspin Turbo 15, 100 kDa cutoff size).

Phase transfer of NPs to D_2O (or a 1:1 volumetric mixture of D_2O and deionized water) using phospholipids. NPs were dispersed in 0.4 mL toluene at 7.0 mg/mL and added with DSPE-mPEG in 0.8 mL chloroform taking appropriate weight ratio of DSPE-mPEG to NP. Chloroform and toluene were completely removed with a rotary evaporator followed by storage under vacuum for 18 h. The NPs were dispersed in 10 mL D_2O (or a 1:1 volumetric mixture of D_2O and deionized water).

Characterization. Transmission electron microscopy (TEM) images were acquired using a JEOL JEM-1400 microscope operating at 80 kV. The NP dispersion in hexane was drop-cast onto a formvar carbon film supported on a 300 mesh copper grid (3 mm in diameter) and

allowed to dry in air at room temperature, before imaging. The size distribution was obtained from averaging a minimum of 250 NPs using ImageJ software (version 1.50i). Electron energy loss spectroscopy (EELS) and Energy-dispersive X-ray spectroscopy (EDX) measurements were done with an Hitachi HF-3300V Scanning Transmission Electron Holography Microscope (STEHM) operated at 200 kV and equipped with EELS (Gatan) and EDX (Bruker) detectors. The NP dispersion in hexane was drop-cast on a lacey carbon grid, dried in vacuum and cleaned in a UV chamber.

X-ray Diffraction (XRD) patterns were collected using a Rigaku Miniflex diffractometer with Cr Kα radiation (λ = 0.2290 nm, 30 kV, 15 mA) with a scan step size of 0.05 degrees (2θ). 15 drops of the NP dispersion in hexane were added onto an indented zero-background sample holder and dried to get the diffraction patterns.

Dynamic light scattering (DLS) measurements were done using a Brookhaven Zeta PALS instrument with a 90Plus/BI-MAS Multi Angle Particle Sizing option, equipped with a 15 mW solid-state laser (658 nm). All data were obtained at a single scattering angle (90^{o}) and averaged over ten scans of the scattered intensity-weighted plots of the NPs dispersed in deionized water, filtered through glass microfiber filter of 0.45 μm pore size (Whatman, Sigma Aldrich) to get rid of dust.

Inductively coupled plasma mass spectroscopy (ICP-MS) analysis was carried out using a Thermo X-Series II (X7) quadrupole ICP-MS to determine the concentration of Eu^{3+}, Gd^{3+} and Y^{3+} ions in the NP stock solution. The aqueous dispersion of NPs was digested in concentrated nitric acid at 135 ^{o}C in sealed Teflon vials for 3 days and diluted with ultrapure water before analysis. Calibration was done by analyzing serial dilutions of a mixed element synthetic standard containing a known amount of europium, gadolinium and yttrium. Each sample, standard and blank, were spiked with indium (to a concentration of ~7 ppb) as the internal standard to correct for signal drift and matrix effects.

Steady state excitation and emission and time resolved lifetime decay measurements were done using an Edinburgh Instruments' FLS920 fluorimeter equipped with a tunable pulsed optical parametric oscillator (OPOTEK Radiant 355 HE 35 LD UVDM), pumped by the third harmonic (355 mm) of the Quantel Q-smart Nd:YAG pump laser. All the emission was collected using a

Hamamatsu R928P PMT (200–700 nm) detector and the spectra were corrected for the instrument sensitivity. All NP dispersions were measured in a 1 cm path length quartz cuvette. Lifetime measurements were done by excitation of Eu^{3+} at 394 nm in the $^5L_6$ level and emission at 615 nm using the OPOTEK Radiant 355 high energy tunable UV-VIS-NIR laser system. A 420 nm short band-pass filter was used to block unwanted scattered wavelengths before the emitted light entered the detector. The data points for lifetime trace of the $^5D_0$ level of the Eu^{3+}-doped NPs were collected over a time range of 80 ms collected in bins of 16 μs. The data were analyzed using OriginPro 2015 (OriginLab, Northampton, MA, version b9.2.272) using relevant first-, second- and third-order exponential decay fittings: $I_t = I_0 e^{-t/\tau_1} + B$, $\frac{I_t}{I_0} = A_1 e^{-t/\tau_1} + A_2 e^{-t/\tau_2} + B$, and $\frac{I_t}{I_0} = A_1 e^{-t/\tau_1} + A_2 e^{-t/\tau_2} + A_3 e^{-t/\tau_3} + B$, where τ_1, τ_2 and τ_3 are the decay lifetime values, I_0 is the intensity at time $t = 0$, B is the background intensity and A_1, A_2 and A_3 denote the pre-exponential factors. The values of τ_1, τ_2 and τ_3 obtained from the exponential fits had statistical uncertainties in the range of 0.001–0.010 ms. The experimental uncertainties were in the range of 0.010–0.100 ms. The average lifetime in case of a biexponential decay was calculated using the equation, $\tau_{av} = \frac{A_1\tau_1^2 + A_2\tau_2^2}{A_1\tau_1 + A_2\tau_2}$ and for a triexponential decay, $\tau_{av} = \frac{A_1\tau_1^2 + A_2\tau_2^2 + A_3\tau_3^2}{A_1\tau_1 + A_2\tau_2 + A_3\tau_3}$.[29] When nonlinear curve fitting was performed using OriginPro 2015, the reduced chi-square was obtained by dividing the residual sum of squares by the degrees of freedom. This quantity is typically not a good measure to determine the goodness of fit because if the *y*-axis data is multiplied by a scaling factor, the reduced chi-square is scaled as well. The r-square value, also known as coefficient of determination gives a good measure of the goodness of fit. If the fit is closer to the data points, the r-square value is closer to 1. Nevertheless, the adjusted r-square value, which accounts for the degrees of freedom, provides a better measure of the goodness of fit than r-square. The adjusted r-square value of all the Eu^{3+} decay curve fittings presented in this article lies in the range 0.99427–0.99939.

Relaxivity measurements. Aqueous dispersions of NPs were used to determine the relaxation times. The T_1 and T_2 measurements were carried out using a 9.4 T/21 cm bore magnet (Magnex, UK) and a Bruker console (Bruker, Germany). A transmit/receive radio frequency volume birdcage coil was applied to excite protons and obtain resonant signal. For the T_2 measurements, a single slice multi-echo pulse sequence was used with the following pulse

parameters: repetition time (TR) 5 s, matrix size 128 × 128, field of view (FOV) 3 cm × 3 cm, slice thickness 2 mm, 128 echoes 4 ms apart. T_2 relaxation times were calculated using a single exponential fitting of the echo train (Marevisi, Canada). For the T_1 measurements, TRUE FISP method was used with the following pulse sequence parameters: TR 3 s, TE 1.5 ms, matrix size 128 × 128, FOV 3 cm × 3 cm, slice thickness 3 mm, 60 frames × 4 segments, segment time 192 ms. The T_1 relaxation times were calculated using single exponential fitting of the data (MATLAB "1sqcurvefit") for different concentrations of NPs in deionized water.

The r_1 and r_2 relaxivities were obtained from the concentration dependent plots of the measured T_1 and T_2 relaxation times in OriginPro 2015 (OriginLab, Northampton, MA, version b9.2.272) using the equation, $\frac{1}{T_i} = \frac{1}{T_i^0} + r_i[Gd^{3+}]; i = 1, 2$, where [$Gd^{3+}$] is the concentration of Gd^{3+} ions in an NP solution obtained from ICP-MS, T_i^0 denote the relaxation times of the water protons in absence of the paramagnetic NPs.

RESULTS AND DISCUSSION

Synthesis and characterization.

Oleate-stabilized $NaGdF_4$, $NaGdF_4$:Eu^{3+} and $NaYF_4$-$NaGdF_4$:Eu^{3+} core-shell NPs were all synthesized in a binary solvent mixture of oleic acid and 1-octadecene following a high temperature route.[11,28] $NaGdF_4$ (including $NaGdF_4$:Eu^{3+}) NPs are known to grow fast.[11] As such, to obtain monodisperse NPs, controlling the nucleation stage in the reaction medium is vital to enable enough nuclei formation to achieve consistent growth of NPs. To obtain $NaYF_4$-$NaGdF_4$:Eu^{3+} core-shell NPs, β-$NaYF_4$ NPs were grown first serving as seeds for the growth of the (Eu^{3+}-doped) $NaGdF_4$ shell. The shell precursor are small (~6 nm diameter) sacrificial α-$NaGdF_4$ NPs possessing cubic phase as revealed from TEM image and XRD analysis in Figure S1 in Supplementary information, respectively. These α-$NaGdF_4$ NPs were injected into the reaction medium with core β-$NaYF_4$ NPs. The growth process proceeds via Ostwald ripening in which larger core particles with smaller surface to volume ratios are favored energetically and grow at the expense of the smaller particles.[28] The NPs dispersed in hexanes were then

transferred to deionized water by coating them with DSPE-mPEG[27] or exchanging the oleate ligands with PVP[26] on their surface which imparted colloidal stability, as illustrated in Figure 1. The as-synthesized NPs have pure hexagonal crystal phase, as confirmed by the XRD patterns of the NPs, which are well indexed with the standard patterns of their corresponding hexagonal phases, β-$NaGdF_4$ and β-$NaYF_4$ (see Figures 2 and S2A). The broad peaks in the XRD pattern of $NaGdF_4$:Eu^{3+} NPs is indicative of the small size of the particles. The peaks for $NaYF_4$-$NaGdF_4$:Eu^{3+} NPs are slightly shifted compared to the standard patterns due to the compressive strain induced by the $NaGdF_4$ shell on the core $NaYF_4$ NPs since ionic radius of Gd (0.938 Å)[30] is slightly larger than that of Y (0.900 Å).[30-31] Figures 3, 4A and S2B show TEM analyses of the three sets of NPs confirming a fairly uniform particle size distribution: β-$NaGdF_4$:Eu^{3+}, β-$NaYF_4$-$NaGdF_4$:Eu^{3+} core-shell and β-$NaGdF_4$ NPs have diameters of 3.0 ± 0.8, 18.8 ± 1.8 and 3.2 ± 0.7 nm, respectively. These average sizes from the TEM images validate the sizes calculated from XRD peaks using the Scherrer equation (see Table S1). Furthermore, Figure S3 shows the TEM image of $NaYF_4$ core NPs before the injection of $NaGdF_4$:Eu^{3+} NPs to form $NaYF_4$-$NaGdF_4$:Eu^{3+} core-shell NPs. The difference in the diameters of the $NaYF_4$ core NPs (Figure S3) and $NaYF_4$-$NaGdF_4$:Eu^{3+} core-shell NPs (Figure 4A) indicates the thickness of the $NaGdF_4$:Eu^{3+} shell which is about 0.5 nm. Electron energy loss spectroscopy (EELS) line scans were acquired across a single β-$NaYF_4$-$NaGdF_4$:Eu^{3+} core-shell NP to provide evidence on the composition of core and shell. Figures S4 (A, B, C) show the high resolution scanning transmission electron microscopy (STEM) image of a single core-shell NP with the corresponding EELS spectrum of the Gd $N_{4,5}$ edge[32] at 140 eV. The signal intensity of Gd changes with position across the particle. The EELS signal intensity of Y in Figure S4B clearly indicates that Y is in the core of the NP while the Gd signal intensity confirms the presence of Gd in the shell. The signal intensity of Eu^{3+} was too low to be resolved. To complement with the EELS data on the structural analyses of the core-shell NP, elemental maps of Y, Gd and Eu acquired from energy dispersive X-ray (EDX) analyses were merged which confirm that Y is located at the core of the particle with Gd in the shell. It further substantiates the presence of Eu^{3+} ions in the shell (see Figures 4 B, C). Inductively coupled plasma mass spectrometry (ICP-MS) was done to obtain the lanthanide ion concentration after digesting the $NaYF_4$-$NaGdF_4$:Eu^{3+} core-shell NPs in concentrated nitric acid. The ionic concentration of Eu^{3+} was found to be 5 atomic % of the total lanthanide (Eu^{3+} and Gd^{3+}) composition in the shell of the NP.

MR relaxivity results.

$NaGdF_4$ NPs are characterized by their longitudinal and transverse relaxivity (r_1 and r_2, respectively), which is the change in relaxation rate ($1/T_1$ and $1/T_2$, respectively) of solvent water protons in presence of the NP, normalized to the concentration of Gd^{3+} ions, [Gd^{3+}], or NPs, as shown in the equation: $\frac{\mathbf{1}}{\boldsymbol{T_i}} = \frac{\mathbf{1}}{\boldsymbol{T_i^0}} + \boldsymbol{r_i}[\boldsymbol{Gd^{3+}}]; \boldsymbol{i = 1, 2}$

To determine Gd^{3+} ionic r_1 and r_2 relaxivities, the Gd^{3+} ion concentration in the dispersions of $NaGdF_4$ NPs coated with PVP and DSPE-mPEG was determined to be 1.15 mM and 1.12 mM in the colloidal dispersion, respectively, using ICP-MS. Gd^{3+} ionic relaxivities (r_1 and r_2) of $NaGdF_4$ and $NaYF_4$-$NaGdF_4$:Eu^{3+} core-shell NPs were obtained from the slope of the linear regression fit in the relaxivity plots obtained at 9.4 T shown in Figure 5 and S5, and the values are tabulated in Table 1. PVP and DSPE-mPEG coated $NaGdF_4$ NPs have r_1 values of 1.77 ± 0.29 mM^{-1} s^{-1} and 1.84 ± 0.01 mM^{-1} s^{-1}, respectively, at 9.4 T. The corresponding r_1 relaxivity values calculated per NP[11]: 443 and 420 mM_{NP}^{-1} s^{-1}. Similarly, PVP and DSPE-mPEG coated $NaYF_4$-$NaGdF_4$:Eu^{3+} core-shell NPs show almost identical Gd^{3+} ionic r_1 relaxivities: 7.27 ± 0.72 mM^{-1} s^{-1} and 6.46 ± 0.35 mM^{-1} s^{-1}, respectively. The corresponding values per NP concentration are 15,800 and 17,500 mM_{NP}^{-1} s^{-1}. Furthermore, PVP and DSPE-mPEG coated $NaGdF_4$ NPs have r_2 values of 14.44 ± 0.59 mM^{-1} s^{-1} and 27.42 ± 0.73 mM^{-1} s^{-1}, respectively. The corresponding r_2 values for $NaYF_4$-$NaGdF_4$:Eu^{3+} core-shell NPs are 52.34 ± 2.53 mM^{-1} s^{-1} and 60.75 ± 2.38 mM^{-1} s^{-1}. We acknowledge the fact that the values for the Eu^{3+}-doped core-shell NPs will be slightly lower than the undoped analogues. However, they may serve nicely as bimodal contrast agents (i.e. MRI and optical contrast). Dynamic light scattering (DLS) results, as shown in Figure S6 and summarized in Table S1, indicate similar hydrodynamic radii for PVP and DSPE-mPEG coated $NaGdF_4$ NPs: 8.9 nm ± 1.9 nm and 8.8 nm ± 1.8 nm, respectively. The hydrodynamic radii for larger sized $NaYF_4$-$NaGdF_4$:Eu^{3+} core-shell NPs coated with PVP and DSPE-mPEG are also close in values: 33.9 ± 1.2 nm and 34.3 nm ± 1.6 nm, respectively. Such close values of thicknesses of the surface coatings of NPs can be related to the similar r_1 (or r_2) relaxivities but these results do not explain the difference between T_1 and T_2 relaxation mechanisms and the role of inner, second, and/or outer spheres of coordination of water molecules, if any, to approach the Gd^{3+} ions on the surface of NPs. In addition, they do not explicitly say much about the characteristics of the surface coatings in terms of assisting with

water accessibility to the surface Gd^{3+} ions on NPs. To understand these relaxation phenomena of Gd^{3+}-based NPs, $NaGdF_4:Eu^{3+}$ and $NaYF_4$-$NaGdF_4:Eu^{3+}$ core-shell NPs were subjected to steady-state and time-resolved measurements to assess the photoluminescence properties of Eu^{3+} ions which are sensitive to proximate water molecules. The photoluminescence lifetime decay of Eu^{3+} ions in NPs enabled us to comprehend the relaxation mechanisms of Gd^{3+} ions in NPs since either of the events are susceptible to the proximity of water molecules to Eu^{3+} and Gd^{3+} ions, respectively.

Steady-state photoluminescence measurements.

In Figure 6, $NaGdF_4:Eu^{3+}$ and $NaYF_4$-$NaGdF_4:Eu^{3+}$ core-shell NPs dispersed in hexanes show emission patterns characteristic of transitions of Eu^{3+} as reported in the past: $^5D_1 - {}^7F_0$ at 525 nm, $^5D_1 - {}^7F_1$ at 535 nm, $^5D_1 - {}^7F_2$ at 554 nm, $^5D_0 - {}^7F_0$ at 578 nm, $^5D_1 - {}^7F_3$ at 582 nm, $^5D_0 - {}^7F_1$ at 591 nm, $^5D_0 - {}^7F_2$ at 615 nm and $^5D_0 - {}^7F_4$ at 680–700 nm.[21,23,33] The excitation wavelength was chosen to be 394 nm because it corresponds to the most intense direct excitation of Eu^{3+} ions. The $^5D_0$ and $^7F_0$ states are non-degenerate implying that only a single Gaussian peak should appear for the $^5D_0 - {}^7F_0$ transition at 578 nm if all the Eu^{3+} ions are in the same crystal site. Deconvolution of the peak centered at 578 nm, obtained with the minimum measurable step size of 0.05 nm, is shown in Figure S7 which reveals three Gaussian peaks indicating the presence of Eu^{3+} ions in more than one symmetry site in the NPs such as the 1*a* and 1*f* sites with C_{3h} symmetry,[34] or the sites of lower symmetry, C_s, C_3, and/or C_1.[35]

Time-resolved photoluminescence measurements.

In the present study, the deconvolution of the $^5D_0 - {}^7F_0$ transition peak suggests the presence of Eu^{3+} ions in more than one crystal site in the $NaGdF_4:Eu^{3+}$ NP lattice. They are in the bulk of the particles away from the surface and on the surface of the particles. As depicted in the crystallographic representation of β-$NaGdF_4$ NP in Figure S8, Eu^{3+} ions (ionic radius = 0.947 Å)[30] can substitute for Gd^{3+} (ionic radius = 0.938 Å)[30] since Eu^{3+} has a slightly larger ionic radius and its occupation at 1*a* and 1*f* sites/Gd^{3+} is favorable energetically.[34] On the other hand,

to occupy the position of larger Na^+ (ionic radius = 1.020 Å)[30] at the expense of more binding energy and charge compensation, e.g., cation vacancy, and/or interstitial defects, it is almost impossible for Eu^{3+} to substitute for Na^+. Thus, Eu^{3+} ions in the "bulk" of the NPs are surrounded by nine F^- ions while those on the surface by a lower number of F^- ions and O (from oleates) or O (from water) depending upon the coordinating ligand. Assuming spherical particles, the model describing the lifetime distribution of a $NaGdF_4$:Eu^{3+} NP can be divided into shells of equal volumes,[36] with Eu^{3+} ions present in the inner shell having a longer lifetime than the outer shell since the core Eu^{3+} ions are devoid of surface quenching effects, especially, in presence of aqueous medium. Similarly, the model describing the lifetime distribution of a $NaYF_4$-$NaGdF_4$:Eu^{3+} core-shell NP can be divided into shells in which the Eu^{3+} ions present on the surface have a shorter lifetime than those penetrating the undoped $NaYF_4$ core. The decay curves for $NaYF_4$-$NaGdF_4$:Eu^{3+} core-shell NPs in hexanes and deuterated water are best fitted using the single exponential equation: $I_t = I_0 e^{-t/\tau_1} + B$. The decay curves of the $NaGdF_4$:Eu^{3+} NPs dispersed in hexanes and deuterated water were fitted using the bi-exponential equation, $\frac{I_t}{I_0} = A_1 e^{-t/\tau_1} + A_2 e^{-t/\tau_2} + B$, while for the both types of NPs dispersed in deionized water or in a mixture of deionized and deuterated water, the tri-exponential equation, $\frac{I_t}{I_0} = A_1 e^{-t/\tau_1} + A_2 e^{-t/\tau_2} + A_3 e^{-t/\tau_3} + B$, was used. The average lifetime in case of a biexponential decay is calculated using the equation, $\tau_{av} = \frac{A_1\tau_1^2 + A_2\tau_2^2}{A_1\tau_1 + A_2\tau_2}$ and for a triexponential decay, $\tau_{av} = \frac{A_1\tau_1^2 + A_2\tau_2^2 + A_3\tau_3^2}{A_1\tau_1 + A_2\tau_2 + A_3\tau_3}$.[29]

Lifetime decay of Eu^{3+}-doped in $NaGdF_4$ NPs (~3 nm diameter; TEM).

The decay of the excited state of Eu^{3+} ions in $NaGdF_4$:Eu^{3+} NPs, dispersed in hexanes, was measured yielding an average lifetime value of 5.23 ms. Following their surface modification with PVP and DSPE-mPEG and then transfer to deionized water, the NPs displayed average lifetime values of 1.74 ms and 1.86 ms, respectively (in Figures 7–8). The average lifetime values are collated in Table 2. Quenching dominates on or near the surface of the NPs when dispersed in water due to vibrational de-excitation of the Eu^{3+} excited state in presence of O–H bond, which is explained as follows. The energy gap between the luminescent state and the

ground state manifold is approximately 12,000 cm^{-1} for Eu^{3+}. The energy gap between the emissive state and the highest lying sublevel of the ground state of Eu^{3+} are effectively spanned by the vibrational modes of O–H oscillators coordinated to Eu^{3+}. The coupling of the Eu^{3+} excited states to the high-frequency vibrational overtones of the O–H bond ($\tilde{\nu}_{O-H}$ = 3,600 cm^{-1}) provides an efficient mechanism for energy transfer, resulting in radiationless de-excitation of the Eu^{3+} ion excited state. The quenching efficiency is sharply decreased in presence of the O–D bond as inferred from the average lifetime values of PVP coated (4.40 ms) and DSPE-mPEG coated (4.19 ms) $NaGdF_4:Eu^{3+}$ NPs dispersed in D_2O (Table 2, Figure 7–8). Coupling to a higher energy overtone, as required for the O–D oscillator ($\tilde{\nu}_{O-D}$ = 2,200 cm^{-1}), results in much less efficient quenching of the Eu^{3+} excited state and, thus, longer-lived Eu^{3+} luminescence. This phenomenon is aptly exhibited by free Eu^{3+} ions [from $Eu(NO_3)_3{\cdot}5H_2O$] when dispersed in D_2O, deionized water or a combination of two (Figure S10). When $Eu(NO_3)_3{\cdot}5H_2O$ is dispersed in deuterated water, deionized water or a mixture of the two (1:1 v/v ratio), the corresponding lifetime values of Eu^{3+} are 2.94 ms, 0.11 ms and 0.24 ms substantiating exchange of water molecules at the Eu^{3+} coordination sites.

When PVP and DSPE-mPEG coated $NaGdF_4:Eu^{3+}$ NPs are dispersed in a 1:1 v/v mixture of deuterated and deionized water, the corresponding values of τ_{av} increase to 2.36 ms (from 1.74 ms in deionized water) and 3.53 ms (from 1.86 ms in deionized water). Such consistent increment of τ_{av} validates varying number of coordinated water molecules to surface Eu^{3+} ions of NPs dispersed in deionized water and a 1:1 v/v mixture of D_2O and H_2O substantiating exchange of the coordinated water molecules on the surface of NPs with the bulk water. These lifetime measurements were repeated after six months using the same batch of NPs in the 1:1 v/v mixture of deuterated and deionized water yielding τ_{av} values of 3.59 ms for PVP coated and 2.61 ms for DSPE-mPEG coated $NaGdF_4:Eu^{3+}$ NPs, as shown in Table 2 and Figure S11. These τ_{av} values (measured after 6 months of NP dispersion) are higher for the NPs dispersed in a 1:1 v/v mixture of deuterated and deionized water than that of the NPs dispersed in deionized water only, evincing water exchange at surface Eu^{3+} sites. Such exchange of water in the inner coordination sphere of Eu^{3+}, despite having a hydrophobic barrier of PVP and DSPE-mPEG, can be ascribed to a "leaky" surface coatings owing to the very high curvature of the 3 nm core sized $NaGdF_4:Eu^{3+}$ NPs that creates loopholes for water accessibility.

Lifetime decay of Eu^{3+} in $NaYF_4$-$NaGdF_4$:Eu^{3+} core-shell NPs (~19 nm diameter; TEM).

The single exponential decay curve of Eu^{3+} in $NaYF_4$-$NaGdF_4$:Eu^{3+} core-shell NPs dispersed in hexanes is shown in Figure S9 which yields an average lifetime value of 5.92 ms owing to minimal quenching effects. When dispersed in deionized water after coating them with PVP and DSPE-mPEG, the NPs display quenched lifetimes, 3.44 ms and 3.76 ms, respectively, after tri-exponential fitting of the decay curves as shown in Figures S12–S13. These vibrational quenching phenomena in deionized water due to overlapping energy levels of Eu^{3+} and O–H are the same as those observed in case of $NaGdF_4$:Eu^{3+} NPs. When $NaYF_4$-$NaGdF_4$:Eu^{3+} core-shell NPs are dispersed in 1:1 v/v mixture of deuterated and deionized water, the average lifetime values were obtained as 3.93 ms and 4.51 ms for PVP coated and DSPE-mPEG coated NPs, respectively. These τ_{av} values do not vary substantially from their corresponding values, 3.44 ms and 3.76 ms, in deionized water. This is contrary to the observations in case of $NaGdF_4$:Eu^{3+} NPs. Such similar lifetime values in deionized water and in a 1:1 v/v mixture of deionized and deuterated water suggests hardly any exchange of water molecules coordinated to the surface Eu^{3+} ions with the bulk in the outer sphere coordination environment. Such an inference of a no, or a very slow water exchange, is further evidenced in the lifetime measurements repeated after six months using the same batch of NPs in the 1:1 v/v mixture of deuterated and deionized water. As shown in Table 2 and Figure S14, post 6 months of their dispersion, PVP coated and DSPE-mPEG coated $NaYF_4$-$NaGdF_4$:Eu^{3+} core-shell NPs display an average lifetime of 3.57 ms and 4.58 ms, respectively, similar to their corresponding values of 3.93 ms and 4.51 ms obtained just after dispersion. Such exchange restraints can be attributed to the dense hydrophobic barrier of PVP and DSPE-mPEG on the surface of the bigger NPs which possess a lower curvature compared to the 3 nm core NP.

In DSPE-mPEG coated $NaYF_4$-$NaGdF_4$:Eu^{3+} core-shell NPs, the methoxy-terminated PEG chains act as the extended hydrophilic head groups for electrostatic interactions and hydrogen bonding with water. In case of PVP coated $NaYF_4$-$NaGdF_4$:Eu^{3+} core-shell NPs, there is an extensive hydrogen bonding among free water molecules and the C–N and C=O group in the pyrrolidone moieties. As depicted in Figure 1, the distearoyl phosphoethanolamine moieties of DSPE-mPEGs interlock with the hydrophobic alkyl chains of oleates on the surface of NPs

via hydrophobic interactions. When coated with PVP, oleate ligands on the NPs are completely exchanged by the PVP molecules.[11] As per DLS results, the hydrodynamic diameter of the DSPE-mPEG and PVP coated $NaYF_4$-$NaGdF_4$:Eu^{3+} core-shell NPs is similar (33.9 and 34.3 nm; Table S1 in Supplementary Information) indicating no marked difference in the thickness of the hydrophobic layer of the coatings of the NPs. The length of PEG2000 chain with a DSPE head, the PEG chain length can be about 2 nm[37] when in mushroom or brush confirmation or it can extend to a maximum length of 15 nm.[38] These values support the DLS results from which a thickness of about 7.5 nm of DSPE-mPEG coating interlocked with oleates around the ~19 nm sized NPs is implied. Previous reports on assessment of water permeability across Mn^{2+} entrapped dipalmitoyl phosphatidylcholine vesicles, employing ^{17}O and ^{1}H NMR, revealed that below 37 ^{o}C, these phospholipids acquire a gel phase.[39] In the gel phase, phospholipids are more or less locked in place and have limited mobility, as a result the water diffusion into the hydrophobic region is highly restricted, owing to the very high activation energy (15 kcal/mol) for water permeation. Hence, at the physiological (37 ^{o}C) and room (25 ^{o}C) temperatures, there is hardly any exchange of water with the bulk in the outer coordination sphere. This is evident from the lifetime value, τ_3, of $NaYF_4$-$NaGdF_4$:Eu^{3+} core-shell NPs dispersed in a mixture of deuterated and deionized water in a volumetric ratio of 1:1 being similar to that in deionized water (Table 2). In D_2O, phospholipids become more compact than in H_2O as D_2O raises the temperature of gel to liquid phase transition resulting in a dry hydrophobic interior. Molecular dynamics simulations have shown that there is a huge difference in the self-diffusion coefficient of H_2O and D_2O molecules hydrating the membrane.[40] Diffusion of D_2O molecules is 43% slower than that of H_2O molecules which leads to hydration of the polar head groups of DSPE-mPEGs including the PEG corona in H_2O in the 1:1 mixture of H_2O and D_2O. Studies have also shown that there is a strong preference for H_2O to hydrate the phospholipids even in a mixture composed of 98:2 D_2O:H_2O; such solvent isotope effect is more pronounced in hydration of a phospholipid than in bulk solvent mixture.[41] In case of PVP coated NPs dispersed in water, although the glass to liquid transition temperature of PVP (M_w = 10,000 Da) is decreased (below 130 ^{o}C),[42] which imparts slight molecular mobility, the polyvinyl moieties entangled with each other create a hydrophobic barrier excluding the water molecules to enter into the inner coordination sphere of Eu^{3+} ions. Because PVP-10 chain can extend to a length of 16 nm,[43] DLS data indicate that the NPs are coated with extended alkyl chains of PVP. In D_2O, the PVP

coating is apparently completely dehydrated and forms a dense packed structure. To infer from the interpretation of the lifetime decays, DSPE-mPEG and PVP coatings around bigger $NaYF_4$-$NaGdF_4$:Eu^{3+} core-shell NPs exclude water molecules from directly exchanging with the ones coordinated with the Eu^{3+} ions on the surface of NPs in the inner coordination sphere. On the contrary, the smaller $NaGdF_4$:Eu^{3+} NPs have adequate exchange of water molecules with the coordinated ones at Eu^{3+} sites on the surface of the NPs.

Lifetime decay based on the priority of choice of a solvent (D_2O or H_2O) for a final dispersion of NPs in 1:1 v/v D_2O:H_2O.

To further show evidence for the predominant contribution of inner and second sphere relaxation in small NPs and outer sphere relaxation in big NPs, the Eu^{3+} lifetime decay was analyzed after adding an equal volume of deionized water to the dispersion of NPs in D_2O and vice versa. As shown in Table S2 and Figure S15, the average lifetime values in the small PVP coated and DSPE-mPEG coated $NaGdF_4$:Eu^{3+} NPs do not change drastically when D_2O was added to the NP dispersion in water or, vice versa. This supports our conclusion of water exchange at the Eu^{3+} sites on the surface of the small NPs consistent with that observed when the NPs were dispersed in a 1:1 v/v mixture of D_2O and H_2O (Table 2). Such water exchange advocates for inner and second sphere contribution in the small NPs.

On the other hand, as seen in Table S2 and Figure S16, the average lifetime values in the big $NaYF_4$-$NaGdF_4$:Eu^{3+} core-shell NPs are quite different when D_2O was added to the NP dispersion in water or, vice versa. The value of τ_{av} is longer when water was added to the PVP coated and DSPE-mPEG coated NPs dispersed in D_2O (4.67 ms and 4.82 ms, respectively, Table S2), than that observed in the NP dispersion in a 1:1 v/v mixture of D_2O and H_2O (3.93 ms and 4.51 ms, respectively, Table 2). This can be explained by the compact and rigid hydrophobic barrier of the surface coating (PVP or DSPE-mPEG) that does not allow water exchange across it. Further, when D_2O was added to the PVP coated and DSPE-mPEG coated NPs dispersed in water, the lifetime values (3.37 ms and 2.94 ms, respectively, Table S2) are smaller than that observed in the NP dispersion in a 1:1 v/v mixture of D_2O and H_2O (3.93 ms and 4.51 ms, respectively, Table 2) and comparable to that of the NP dispersion in water (3.44 ms and 3.76

ms, respectively, Table 2). This is consistent with a slow or negligible water exchange across the hydrophobic barrier surrounding the NPs from the bulk solvent which, thus, suffices for the outer sphere contribution in the big NPs.

Contribution of inner, second, and outer spheres of relaxation of water protons towards NP relaxivities.

High-field regime relaxation ($B_0 \geq 3$ T). Relaxivities r_i (i = 1, 2) of an NP are the sum of the inner sphere (IS), second sphere (2S) and outer sphere (OS) contributions from the water proton dynamics with respect to the NP, $r_i = r_i^{IS} + r_i^{2S} + r_i^{OS}$. A schematic representation of these contributions from the water protons with respect to an NP is depicted in Figure 9. The relaxivity equations discussed below for IS, 2S and OS of relaxation are from the Grenoble method.[44-45] In the high-field domain ($B_0 \geq 3$ T), the relaxivities are independent of the electronic spin relaxation.[2,17]

High-field inner and second sphere relaxation. The IS relaxivity is proportional to the number q of water molecules coordinated to the surface Gd^{3+} ions of NP and decreases rapidly with the mean distance r_H between NP (Gd^{3+}) and water proton distance as $1/r_H^6$. It is a function of the mean residence time of the coordinated water molecules τ_M and Brownian motion of the NP characterized by a tumbling time or a rotation correlation time of r_r. The IS relaxivity is given by

$$r_i^{IS} = Pq/(T_{iM} + \tau_M),$$

where i = 1, 2; P is the ratio of the number of NPs to number of water molecules in a 1 mM solution, T_{iM} are the relaxation times of the protons of water molecules coordinated directly to the NP which are given by[44]

$$\frac{1}{T_{1M}} = A\frac{1}{4\pi r_H^6}\frac{\tau_r}{1+\omega_I^2\tau_r^2}$$

$$\frac{1}{T_{2M}} = A\frac{\tau_r}{4\pi r_H^6}\left[\frac{2}{3}+\frac{1}{2}\frac{1}{1+\omega_I^2\tau_r^2}\right]$$

where, $A = \left(\frac{\mu_0}{4\pi}\right)^2 (\frac{8\pi}{5})\gamma_I^2\mu_{eff}^2$ and $\mu_{eff} = g_S\mu_B[S(S+1)]^{1/2}$, g_S is the Landé factor of the electronic spin S, γ_I and γ_S ($= -g_S\mu_B/\hbar$) are the gyromagnetic ratios of the interacting spins I

and S through the dipolar coupling factor μ_0 is the permeability of vacuum, and ω_I and ω_S are the angular Larmor frequencies of the spins such that $\omega_I = 2\pi\nu_I = -\gamma_I B_0$ and $\omega_S = -\gamma_S B_0$.

The Eu^{3+} lifetime analyses of PVP and DSPE-mPEG coated $NaGdF_4$:Eu^{3+} NPs manifested adequate exchange of water molecules with the coordinated ones at Eu^{3+} sites on the surface of these small NPs. This implies the direct access and coordination of water protons to the surface Gd^{3+} ions of the smaller NPs clearly showing the dominance of the inner sphere relaxation mechanism. Further, the contribution from the second sphere (2S) is obvious from the fact that a realistic model considers the 2S longitudinal and transverse relaxivities r_i^{2S} resulting from hydrogen bonding of the water molecules to the sites on the NP surface coating, for example, C=O and >N– sites in PVP and C=O, –NH– sites and PO_4 moiety in DSPE-mPEG, in which the water molecules are at different distances from the surface Gd^{3+} ions of the NP. The high field 2S relaxivity equations are simplified to follow the parameters similar to those in IS relaxivity equations because, ideally, there are many parameters involved in the 2S relaxivity description and their determination is beyond the scope of obtaining all experimental information from all possible available techniques. The 2S relaxivities, $r_i^{2S} = Pq'/(T'_{iM} + \tau'_{iM})$, where T'_{iM} are the relaxation times of the protons of 2S water molecules and the number of 2S water molecules is q', with effective residence time τ'_M and the effective distance between these water protons and NP is r'_H. The 2S relaxivities are given by[17]

$$\frac{1}{T'_{1M}} = A\frac{1}{4\pi r_H'^6}\frac{\tau'_c}{1+\omega_I^2\tau_c'^2}$$

$$\frac{1}{T'_{2M}} = A\frac{\tau'_c}{4\pi r_H'^6}\left[\frac{2}{3}+\frac{1}{2}\frac{1}{1+\omega_I^2\tau_c'^2}\right]$$

where the 2S correlation time τ'_c is given by

$$\frac{1}{\tau'_c} = \frac{1}{\tau_r} + \frac{1}{\tau'_M}$$

High-field outer sphere relaxation. OS relaxivity theory is based on the OS dipolar time correlation function $g_2(t)$. Suppose **r** is the vector joining the nuclear spin I of a water molecule M_I to the electronic spin S of Gd^{3+} ions in the NP and (r, θ, ϕ) are spherical coordinates in the

laboratory (L) frame, the z axis of which is parallel to $\mathbf{B}_0$. Let $Y_{2q}(\theta, \phi)$ ($-2 \leq q \leq 2$) be the spherical harmonics of order 2. The function $g_2(t)$ of the random functions $r^{-3}Y_{2q}(\theta, \phi)$ of the interspin vector $\mathbf{r}$, independent of the index q, is defined as[2,46]

$$g_2(t) = N_S \iint \frac{Y_{2q}(\theta_0, \phi_0)}{r_0^3} \frac{Y_{2q}^*(\theta, \phi)}{r^3} g_{site\ I-site\ S}^{OS}(r_0) \rho(\mathbf{r}_0, \mathbf{r}, t) \mathrm{d}\mathbf{r}_0 d\mathbf{r}$$

where N_S is the number of electron spins S or Gd^{3+} ions per unit volume, $g_{site\ I-site\ S}^{OS}(r_0)$ is the radial distribution function of the interspin distance r_0 at equilibrium and $\rho(\mathbf{r}_0, \mathbf{r}, t)$ is the OS propagator describing the random evolution of the interspin vector $\mathbf{r}$ in the course of time. In other words, $\rho(\mathbf{r}_0, \mathbf{r}, t)$ is the conditional probability that the interspin position is $\mathbf{r} \equiv (r, \theta, \phi)$ at time t given that it was at $\mathbf{r}_0 \equiv (r_0, \theta_0, \phi_0)$ at initial time $t = 0$. $\rho(\mathbf{r}_0, \mathbf{r}, t)$ is governed by the anisotropic translational and rotational Brownian motions of water protons and NPs without binding to the water molecules. The translational correlation time τ_d characterizes the time decay of $g_2(t)$ and is defined as $\tau_d = a^2/D$, where a is the average of all the closest inter-center distance between NP and water proton for a given relative orientation of the two, over all their possible orientations, and D is the relative diffusion coefficient which is the sum of the self-diffusion coefficients of water proton and NP, $D = D_{M_I}^t + D_{NP}^t$. In case of an NP, its hydrodynamic radius is the distance of closest approach a of the water proton to the surface Gd^{3+} ions since an NP on its whole impacts on the relaxation of water protons. The dipolar spectral density is the Fourier transform of $g_2(t)$ defined as $j_2(\omega) = \int_0^\infty g_2(t) \cos(\omega t)\, dt$ and given by

$$j_2(\omega) = \frac{N_S}{Da} Re\left[\frac{4 + x}{3(9 + 9x + 4x^2 + x^3)}\right]$$

where $x = \sqrt{i\omega\tau_d}$. The OS relaxivities are linear combinations of spectral density $j_2(\omega)$ of $g_2(t)$, and given by $r_1^{OS} = A j_2(\omega_I)$ and $r_2^{OS} = A\left[\frac{2}{3} j_2(0) + \frac{1}{2} j_2(\omega_I)\right]$

In case of PVP and DSPE-mPEG coated $NaYF_4$-$NaGdF_4$:Eu^{3+} core-shell NPs, the Eu^{3+} lifetime decay analyses of the doped Eu^{3+} ions conveyed about the hydrophobic barrier around the NP that debars the access and exchange of water molecules with the ones coordinated to the surface Eu^{3+} ions of NPs in the inner coordination sphere. This suggests no water coordination, exchange or accessibility to the surface Gd^{3+} ions of the NPs indicating the dominance of outer

sphere relaxation mechanism. This is consistent with the O-17 and H-1 NMR studies by us and collaborators which demonstrate exclusive contribution of the outer sphere relaxation towards the relaxivities of oleic acid/poly(maleic anhydride-*alt*-1-octadecene)−polyethylene glycol coated Ln^{3+}-based core-shell NPs (diameters in the range of 16.5–20.5 nm).[47]

The difference in the hydrodynamic diameter obtained from DLS and diameter of NPs determined from histograms developed from the corresponding TEM images gives the thickness of the hydrophobic barrier between the surface Gd^{3+} sites of NPs and the water protons. From Table S1, the hydrophobic layer is ~15 nm thick in both PVP and DSPE-mPEG coated $NaYF_4$-$NaGdF_4$:Eu^{3+} core-shell NPs indicating almost equal contribution from the OS relaxation. This is in agreement with the corresponding close values of r_1 relaxivities 15,800 and 17,500 mM_{NP}^{-1} s^{-1} per NP concentration (Gd^{3+} ionic relaxivities are 7.27 and 6.46 mM^{-1} s^{-1}) and r_2 relaxivities 115,200 and 114,200 mM_{NP}^{-1} s^{-1} per NP concentration (Gd^{3+} ionic relaxivities are 52.34 and 60.75 mM^{-1} s^{-1}). The difference in the r_1 and r_2 relaxivities ($r_1 < r_2$) of an NP comes largely from the spectral density terms $j_2(0)$ and $j_2(\omega_I)$.

The contribution of Curie relaxivity in the inner and outer spheres of relaxation has been discussed in published works.[4,48] Curie relaxation arises from the interaction of the fluctuating local magnetic fields at the position of the studied nuclear spin I with the various average magnetic moments of the spins S of the Gd^{3+} ions. The Curie correction factor is given by[17]

$$\varepsilon_{Curie} \equiv \frac{1}{3} S(S+1) \left(\frac{g_S \mu_B B_0}{k_B T} \right)^2$$

At magnetic field $B_0 \leq 10$ T at room temperature, the Curie correction factor, ε_{Curie}, which varies with field as B_0^2, is smaller than 1 %. As such, the Curie relaxivities can be neglected. $r_i^{total} = r_i + \varepsilon_{Curie} r_i = (1 + \varepsilon_{Curie}) r_i \cong r_i$

From the comprehensive analyses of Eu^{3+} lifetime decays, it is conclusive that at an applied magnetic field ≥ 3 T, the smaller $NaGdF_4$:Eu^{3+} NPs have a dominant contribution from the inner and second spheres towards their relaxivities while the larger $NaYF_4$-$NaGdF_4$:Eu^{3+} core-shell NPs have a predominant contribution from outer sphere relaxation of water protons with respect to the surface Gd^{3+} ions of the NPs.

CONCLUSIONS

In conclusion, to understand the qualitative contribution of inner, second, and outer spheres of T_1 and T_2 relaxation mechanisms of water protons with respect to water dispersed Gd^{3+}-based NPs at a magnetic field of 9.4 T, systematic investigation on europium decay curves of $NaGdF_4:Eu^{3+}$ and $NaYF_4$-$NaGdF_4:Eu^{3+}$ core-shell NPs have been carried out. Inner and second sphere contributions have been proved to be predominant towards r_1 and r_2 relaxivities of the smaller $NaGdF_4$ NPs (3 nm diameter) owing to the "leaky" coatings on the high curvature NP surface and easy accessibility and exchange of water protons with the ones coordinated directly to the surface Eu^{3+} or Gd^{3+} ions. On the other hand, outer sphere contribution governs the relaxivities in the larger $NaYF_4$-$NaGdF_4:Eu^{3+}$ core-shell NPs (18.3 nm core diameter with 0.5 nm thick shell) since the hydrophobic barrier on the low curvature NP surface forbids water accessibility to the surface Eu^{3+} or Gd^{3+} ions. The r_1 values of $NaGdF_4$ NPs were found to be almost identical for either type of surface coatings of PVP and DSPE-mPEG at 9.4 T. Similar observations were made for the r_1 and r_2 relaxivities of $NaYF_4$-$NaGdF_4:Eu^{3+}$ core-shell NPs. The very many parameters, such as the time periods of different exchange processes and residence of water protons at the surface of a NP, translational correlation time, and spectral density terms, governing the inner, second, and outer sphere relaxation mechanisms of a paramagnetic ion/Gd^{3+}-based NP need to be well understood to design NPs with optimal relaxivities to obtain MR image with high contrast to noise ratio for efficient medical diagnosis.

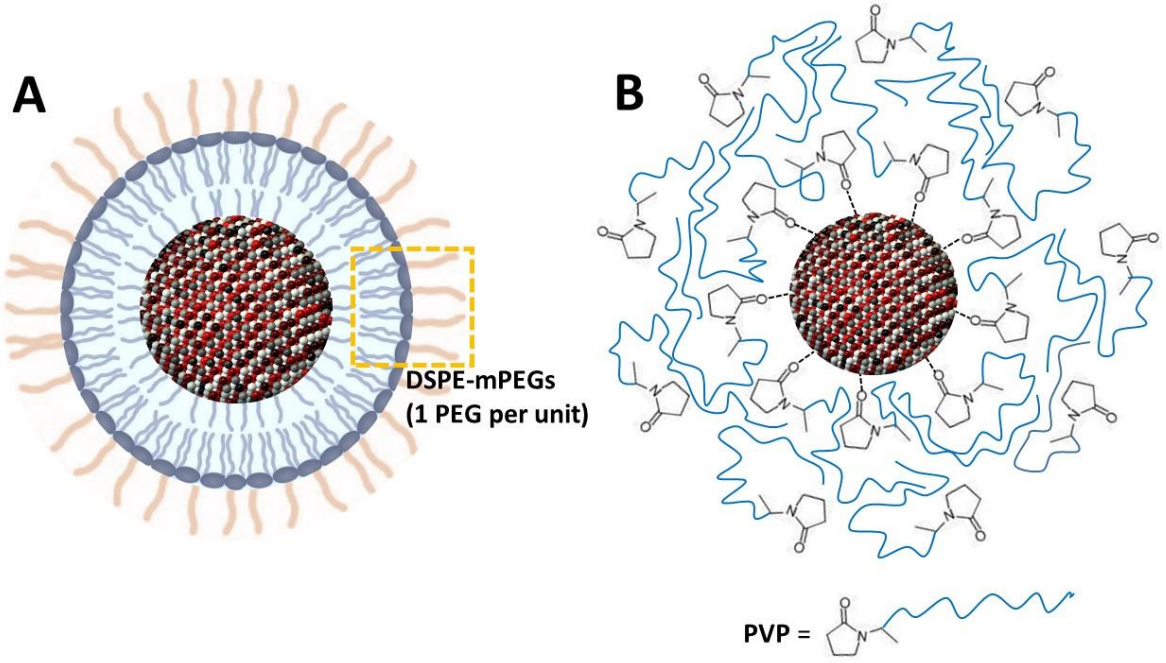

Figure 1. Schematic representation of NPs coated with (A) DSPE-mPEG and (B) PVP. A hydrophobic barrier is formed when the oleate chains on NPs interlock with the alkyl moieties of DSPE-mPEGs. In case of PVP coated NPs, the C=O group of the pyrrolidone ring coordinates to metal cations on the surface of the NPs while the polyvinyl moieties organize in a densely compact structure due to hydrophobic interaction. The C=O groups of the PVP coating, which are not bonded to the metal cations, coordinate to water molecules via hydrogen bonding.

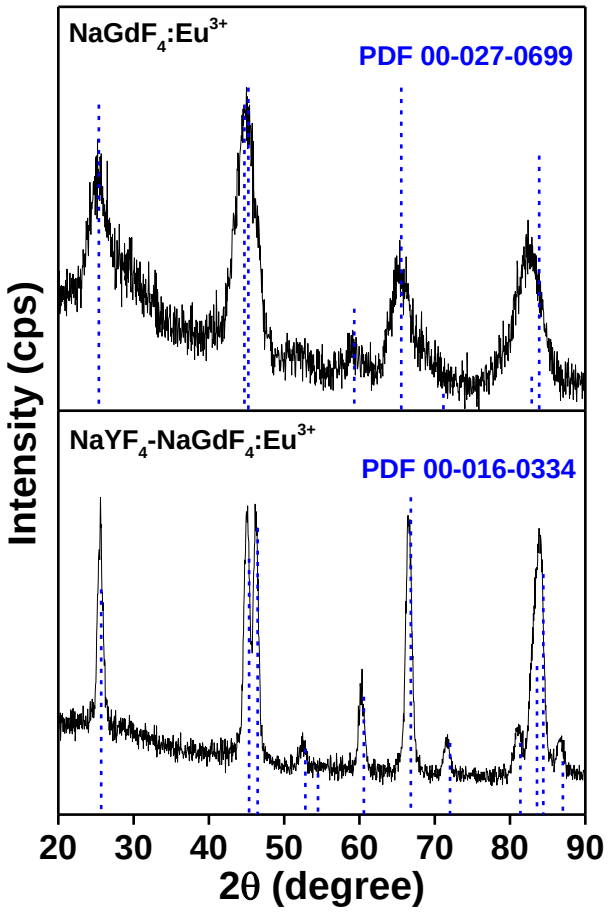

Figure 2. XRD patterns of $NaGdF_4:Eu^{3+}$ and $NaYF_4$-$NaGdF_4:Eu^{3+}$ core-shell NPs indexed with the corresponding standard patterns of the hexagonal phase of $NaGdF_4$ (PDF 00-027-0699) and $NaYF_4$ (PDF 00-016-0334).

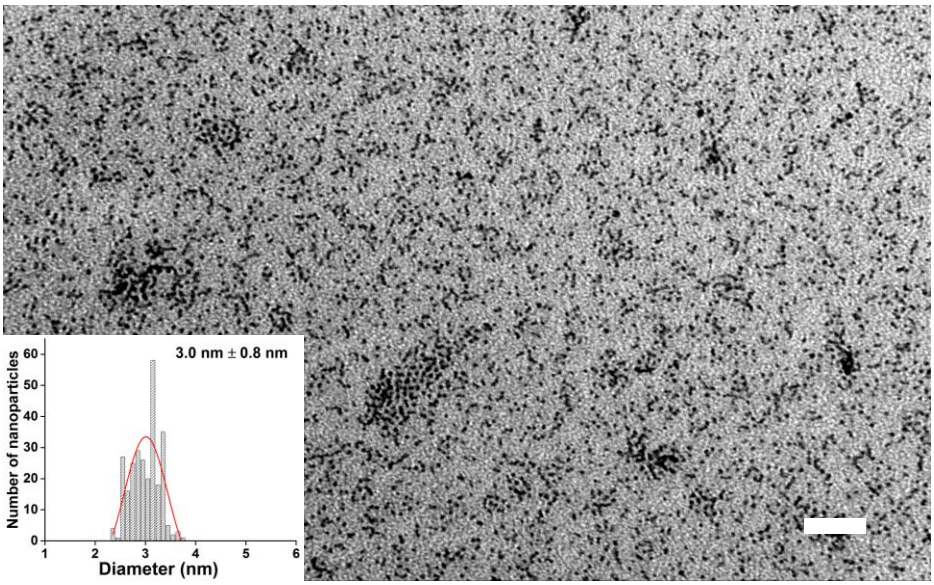

Figure 3. $NaGdF_4:Eu^{3+}$ NPs: TEM image (white scale bar: 50 nm) and the corresponding histogram of particle size distribution.

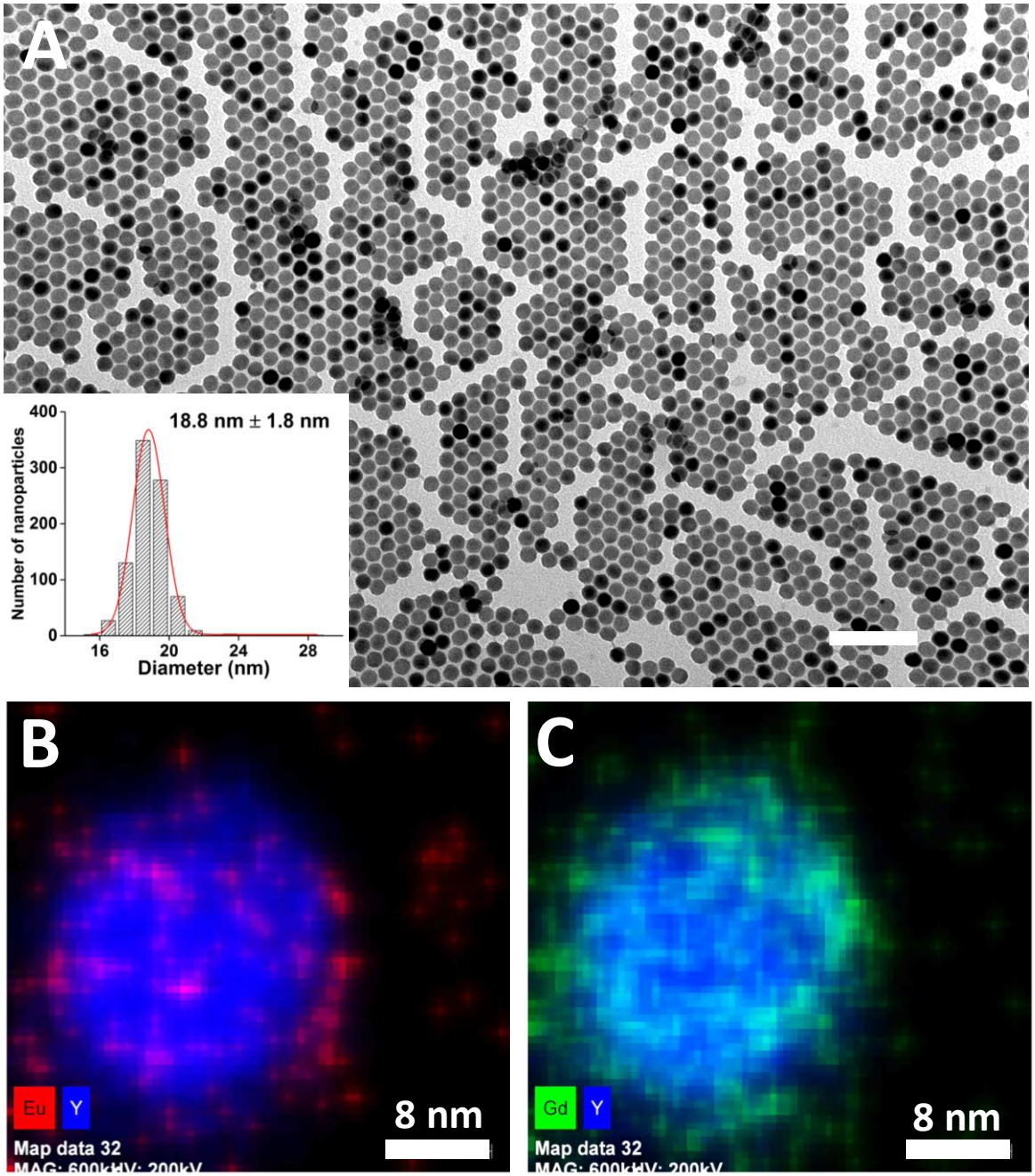

Figure 4. $NaYF_4$-$NaGdF_4$:Eu^{3+} core-shell NPs: (A) TEM image (white scale bar: 100 nm) and the corresponding histogram of particle size distribution. Single particle elemental maps from EDX analyses on STEHM in which (B) Y (blue) and Eu (red) maps are merged and (C) Y (blue) and Gd (green) maps are merged.

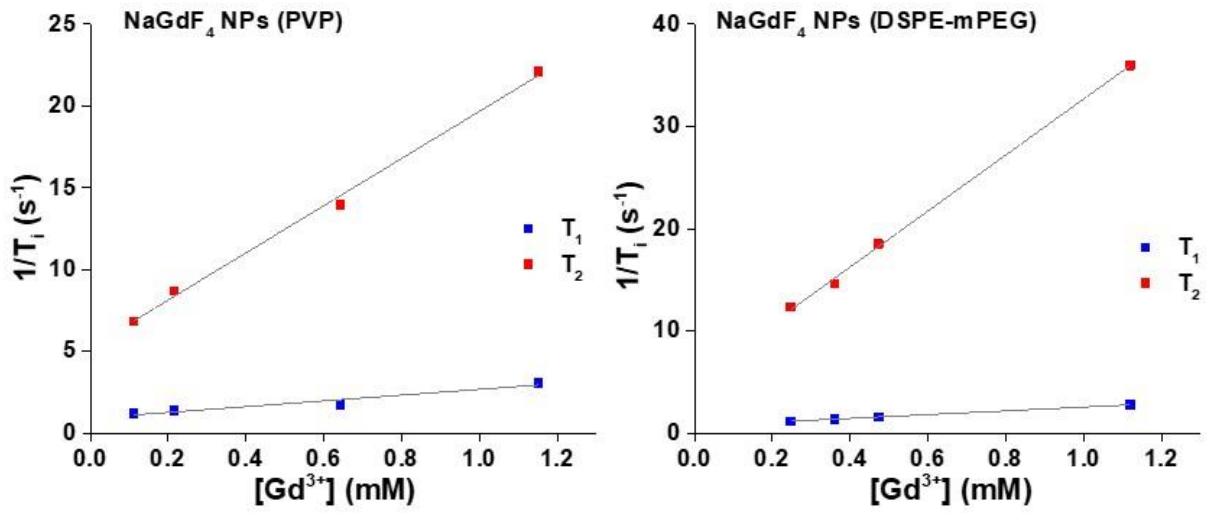

Figure 5. Longitudinal (r_1) and transverse (r_2) relaxivities obtained for PVP and DSPE-mPEG coated $NaGdF_4$ NPs at 9.4 T.

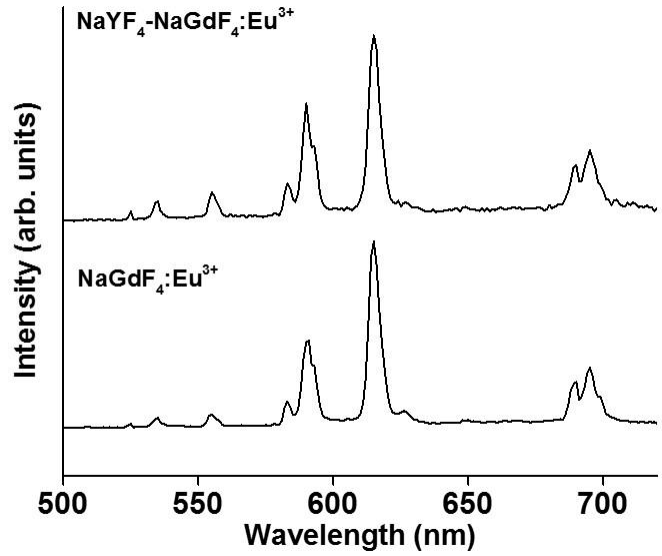

Figure 6. Emission spectra of $NaGdF_4:Eu^{3+}$ NPs and $NaYF_4$-$NaGdF_4:Eu^{3+}$ core-shell NPs dispersed in hexanes. The NPs were excited at 394 nm.

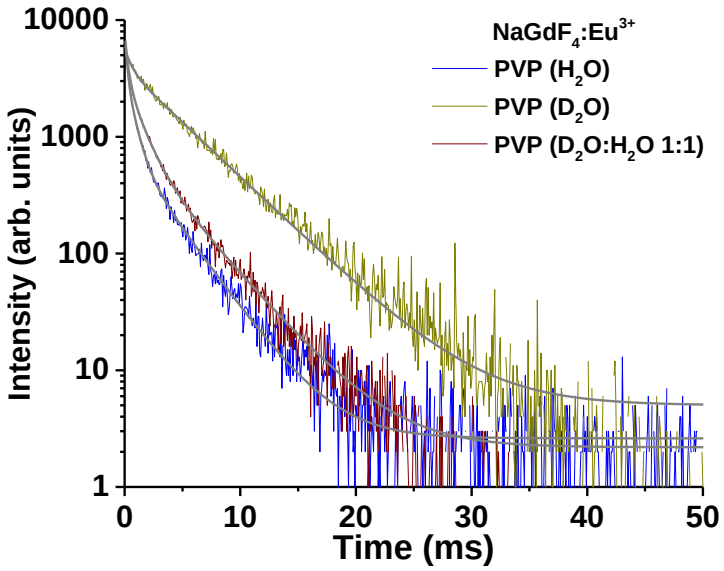

Figure 7. Decay curves monitored at 615 nm and fitted with corresponding exponential equations for $NaGdF_4:Eu^{3+}$ NPs coated with PVP and dispersed in D_2O and/or H_2O. The NPs were excited at 394 nm. R-squared (COD) for the curves is in the range of 0.99539–0.99937.

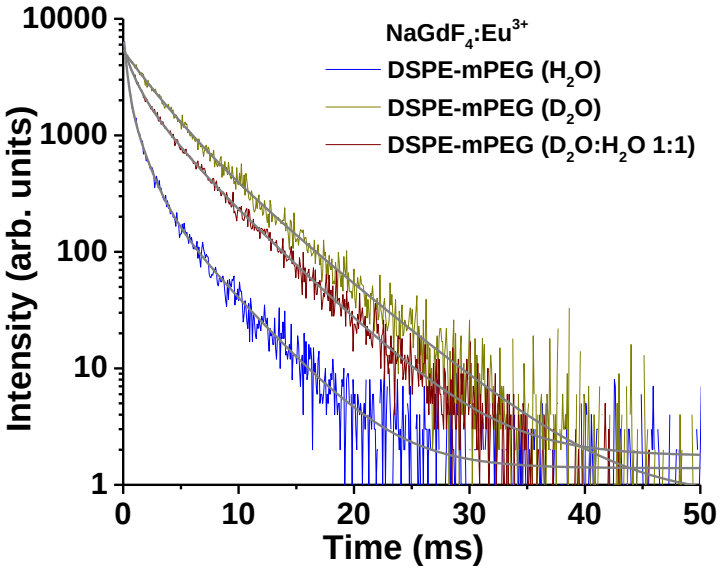

Figure 8. Decay curves monitored at 615 nm and fitted with corresponding exponential equations for $NaGdF_4:Eu^{3+}$ NPs coated with DSPE-mPEG and dispersed in D_2O and/or H_2O. The NPs were excited at 394 nm. R-squared (COD) for the curves is in the range of 0.99753–0.99904.

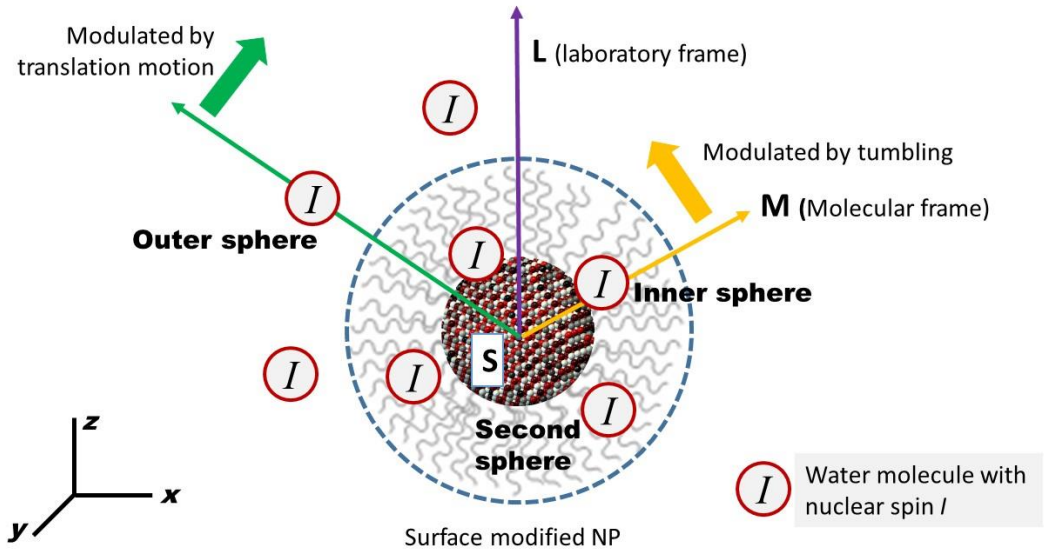

Figure 9. Schematic representation of contributions from inner, second, and outer spheres of relaxation of water protons towards relaxivities of an NP. Dipole-dipole interaction is between electron spin (S) of Gd^{3+} ion ensemble in NP and nuclear spin (I) of water molecule.

Table 1. r_1 and r_2 relaxivities for β-$NaGdF_4$ and $NaYF_4$-$NaGdF_4$:Eu^{3+} core-shell NPs with different surface coatings at 9.4 T.

NP type	**NP surface coating**	**Ionic relaxivity r_1/[Gd^{3+}] (mM^{-1} s^{-1})**	**Ionic relaxivity r_2/[Gd^{3+}] (mM^{-1} s^{-1})**	**Ionic relaxivity ratio r_2/r_1**	**NP relaxivity r_1/NP (mM_{NP}^{-1} s^{-1})**	**NP relaxivity r_2/NP (mM_{NP}^{-1} s^{-1})**
$NaGdF_4$	PVP	1.77 ± 0.29	14.44 ± 0.59	8.15	443	3443
	DSPE-mPEG	1.84 ± 0.01	27.42 ± 0.73	14.90	420	6263
$NaYF_4$-$NaGdF_4$:Eu^{3+}	PVP	7.27 ± 0.72	52.34 ± 2.53	7.20	15,800	115,200
	DSPE-mPEG	6.46 ± 0.35	60.75 ± 2.38	9.40	17,500	114,200

Table 2. Average lifetime values (τ_{av}) obtained from the exponential decay curves monitored at 615 nm.

Sample	Surface coating	Solvent	τ_{av} (ms)	Sample	Surface coating	Solvent	τ_{av} (ms)
$NaGdF_4:Eu^{3+}$ NPs	Oleic acid	Hexanes	5.23	$NaYF_4$-$NaGdF_4:Eu^{3+}$ core-shell NPs	Oleic acid	Hexanes	5.92
	PVP	D_2O	4.40		PVP	D_2O	6.14
		Deionized water	1.74			Deionized water	3.44
		D_2O : Deionized water 1:1	2.36			D_2O : Deionized water 1:1	3.93
		D_2O : Deionized water 1:1 (6 months after)	3.59			D_2O : Deionized water 1:1 (6 months after)	3.57
	DSPE-mPEG	D_2O	4.19		DSPE-mPEG	D_2O	6.57
		Deionized water	1.86			Deionized water	3.76
		D_2O : Deionized water 1:1	3.53			D_2O : Deionized water 1:1	4.51
		D_2O : Deionized water 1:1 (6 months after)	2.61			D_2O : Deionized water 1:1 (6 months after)	4.58
$Eu(NO_3)_3 \cdot 5H_2O$		D_2O	2.94				
		Deionized water	0.11				
		D_2O : Deionized water 1:1	0.24				

The values of τ_{av} determined from the exponential fits had statistical uncertainties in the range of 0.001–0.010 ms. The experimental uncertainties were in the range of 0.010–0.200 ms.

ASSOCIATED CONTENT

Supporting Information. XRD, TEM, histograms of particle size distribution of α- and β-$NaGdF_4$ NPs. TEM of core $NaYF_4$ NPs before injecting $NaGdF_4:Eu^{3+}$ NPs to form $NaYF_4$-$NaGdF_4:Eu^{3+}$ core-shell NPs. EELS of $NaYF_4$-$NaGdF_4:Eu^{3+}$ core-shell NPs. Relaxivity plots, r_1 and r_2, of $NaYF_4$-$NaGdF_4:Eu^{3+}$ core-shell NPs. DLS plots of $NaGdF_4$, $NaGdF_4:Eu^{3+}$ and $NaYF_4$-$NaGdF_4:Eu^{3+}$ core-shell NPs. Table of sizes of $NaGdF_4$, $NaGdF_4:Eu^{3+}$ and $NaYF_4$-$NaGdF_4:Eu^{3+}$ core-shell NPs from XRD, TEM and DLS. Deconvolution of the emission spectra of $NaGdF_4:Eu^{3+}$ and $NaYF_4$-$NaGdF_4:Eu^{3+}$ core-shell NPs at 578 nm obtained with step size of 0.05 nm. Crystallographic representation of hexagonal phase of $NaGdF_4:Eu^{3+}$ NP. Decay curves of $NaGdF_4:Eu^{3+}$ and $NaYF_4$-$NaGdF_4:Eu^{3+}$ core-shell NPs in hexanes. Decay curves of $NaGdF_4:Eu^{3+}$ and $NaYF_4$-$NaGdF_4:Eu^{3+}$ core-shell NPs measured after 6 months of sample preparation in 1:1 v/v mixture of D_2O and H_2O. Lifetimes values and decay curves when deionized water is added to the NP dispersion in D_2O and vice versa. This material is available free of charge via the Internet at http://pubs.acs.org.

AUTHOR INFORMATION

Corresponding Author

*fvv@uvic.ca

ACKNOWLEDGMENT

We thank the Natural Sciences and Engineering Research Council (NSERC) of Canada and the Alberta Innovates – Health Solutions for funding. We acknowledge Dr. Jody Spence (University of Victoria) for ICP-MS analyses. We also thank the Advanced Microscopy Facility (University of Victoria) for EELS and EDX measurements on STEHM.

REFERENCES

1. Mansfield, P. Snapshot Magnetic Resonance Imaging (Nobel Lecture). *Angew. Chem. Int. Ed.* **2004**, *43*, 5456–5464.
2. Merbach, A. E.; Toth, E. The Chemistry of Contrast Agents in Medical Magnetic Resonance Imaging. John Wiley & Sons Ltd., Chichester (UK): 2001.
3. Caravan, P. Strategies for Increasing the Sensitivity of Gadolinium based MRI Contrast Agents. *Chem. Soc. Rev.* **2006**, *35*, 512–523.
4. Norek, M.; Peters, J. A. MRI Contrast Agents based on Dysprosium or Holmium. *Nucl. Magn. Reson. Spec.* **2011**, *59*, 64–82.
5. Blasiak, B.; Landry, J.; Tyson, R.; Sharp, J.; Iqbal, U.; Abulrob, A.; Rushforth, D.; Matyas, J.; Ponjevic, D.; Sutherland, G. R., *et al.* Molecular Susceptibility Weighted Imaging of the Glioma Rim in a Mouse Model. *J. Neurosc. Meth.* **2014**, *226*, 132–138.
6. Blasiak, B.; Barnes, S.; Foniok, T.; Rushforth, D.; Matyas, J.; Ponjevic, D.; Weglarz, W. P.; Tyson, R.; Iqbal, U.; Abulrob, A., *et al.* Comparison of T2 and T2*-weighted MR Molecular Imaging of a Mouse Model of Glioma. *BMC Med. Imaging* **2013**, *13*, 20–28.
7. Caravan, P.; Farrar, C. T.; Frullano, L.; Uppal, R. Influence of Molecular Parameters and Increasing Magnetic Field Strength on Relaxivity of Gadolinium- and Manganese-based T_1 Contrast Agents. *Contrast Media Mol. Imaging* **2009**, *4*, 89–100.
8. Caravan, P.; Ellison, J. J.; McMurry, T. J.; Lauffer, R. B. Gadolinium(III) Chelates as MRI Contrast Agents: Structure, Dynamics and Applications. *Chem. Rev.* **1999**, *99*, 2293–2352.
9. Bridot, J. L.; Faure, A. C.; Laurent, S.; Riviere, C.; Billotey, C.; Hiba, B.; Janier, M.; Josserand, V.; Coll, J. L.; Vander Elst, L., *et al.* Hybrid Gadolinium Oxide Nanoparticles: Multimodal Contrast Agents for In Vivo Imaging. *J. Am. Chem. Soc.* **2007**, *129*, 5076−5084.
10. Das, G. K.; Johnson, N. J. J.; Cramen, J.; Blasiak, B.; Latta, P.; Tomanek, B.; van Veggel, F. C. J. M. $NaDyF_4$ Nanoparticles as T_2 Contrast Agents for Ultrahigh Field Magnetic Resonance Imaging. *J. Phys. Chem. Lett.* **2012**, *3*, 524−529.
11. Johnson, N. J. J.; Oakden, W.; Stanisz, G. J.; Prosser, R. S.; van Veggel, F. C. J. M. Size-Tunable, Ultra-Small $NaGdF_4$ Nanoparticles: Insights into their T_1 MRI Contrast Enhancement. *Chem. Mater.* **2011**, *23*, 3714–3722.
12. Zhang, X.; Blasiak, B.; Marenco, A. J.; Trudel, S.; Tomanek, B.; van Veggel, F. C. J. M. Design and Regulation of $NaHoF_4$ and $NaDyF_4$ Nanoparticles for High-Field Magnetic Resonance Imaging. *Chem. Mater.* **2016**, *28*, 3060−3072.
13. Vaughan, T.; DelaBarre, L.; Snyder, C.; Tian, J.; Akgun, C.; Shrivastava, D.; Liu, W.; Olson, C.; Adriany, G.; Strupp, J., *et al.* 9.4T Human MRI: Preliminary Results. *Magn. Reson. Med.* **2006**, *56*, 1274–1282.
14. Kemper, V. G.; Martino, F. D.; Emmerling, T. C.; Yacoub, E.; Goebel, R. High Resolution Data Analysis Strategies for Mesoscale Human Functional MRI at 7 and 9.4T. *NeuroImage* **2017**, *164*, 48–58.
15. Bihan, D. L.; Schild, T. Human Brain MRI at 500 MHz, Scientific Perspectives and Technological Challenges. *Supercond. Sci. Technol.* **2017**, *30*, 033003.
16. Vaughan, J. T.; Snyder, C. J.; DelaBarre, L. J.; Bolan, P. J.; Tian, J.; Bolinger, L.; Adriany, G.; Andersen, P.; Strupp, J.; Ugurbil, K. 7 T Whole Body Imaging: Preliminary Results. *Magn Reson Med.* **2009**, *61*, 244–248
17. Bonnet, C. S.; Fries, P. H.; Crouzy, S.; Delangle, P. Outer-Sphere Investigation of MRI Relaxation Contrast Agents. Example of a Cyclodecapeptide Gadolinium Complex with Second-Sphere Water. *J. Phys. Chem. B* **2010**, *114*, 8770–8781.

18. Bonnet, C. S.; Fries, P. H.; Crouzy, S.; Seneque, O.; Cisnetti, F.; Boturyn, D.; Dumy, P.; Delang, P. A Gadolinium-Binding Cyclodecapeptide with a Large High-Field Relaxivity Involving Second-Sphere Water. *Chem. Eur. J.* **2009**, *15*, 7083–7093.
19. Helm, L. Relaxivity in Paramagnetic Systems: Theory and Mechanisms. *Prog. Nucl. Magn. Reson. Spec.* **2006**, *49*, 45–64.
20. Koenig, S. H.; Kellar, K. E. Theory of $1/T_1$ and $1/T_2$ NMRD Profiles of Solutions of Magnetic Nanoparticles. *Magn. Reson. Med.* **1995**, *34*, 227–233.
21. Bűnzli, J.-C. G. Lanthanide Luminescence for Biomedical Analyses and Imaging. *Chem. Rev.* **2010**, *110*, 2729–2755.
22. Dong, H.; Du, S.-R.; Zheng, X.-Y.; Lyu, G.-M.; Sun, L.-D.; Li, L.-D.; Zhang, P.-Z.; Zhang, C.; Yan, C.-H. Lanthanide Nanoparticles: From Design toward Bioimaging and Therapy. *Chem. Rev.* **2015**, *115*, 10725−10815.
23. Bűnzli, J.-C. G.; Piguet, C. Taking Advantage of Luminescent Lanthanide ions. *Chem. Soc. Rev.* **2005**, *34*, 1048–1077.
24. Kattel, K.; Park, J. Y.; Xu, W.; Kim, H. G.; Lee, E. J.; Bony, B. A.; Heo, W. C.; Lee, J. J.; Jin, S.; Baeck, J. S., *et al.* A Facile Synthesis, In vitro and In vivo MR Studies of D-Glucuronic Acid-Coated Ultrasmall Ln_2O_3 (Ln = Eu, Gd, Dy, Ho, and Er) Nanoparticles as a New Potential MRI Contrast Agent. *ACS Appl. Mater. Interfaces* **2011**, *3*, 3325–3334.
25. Sudarsan, V.; van Veggel, F. C. J. M.; Herring, R. A.; Raudsepp, M. Surface Eu^{3+} Ions are Different than ‘‘Bulk’’ Eu^{3+} Ions in Crystalline Doped LaF_3 Nanoparticles. *J. Mater. Chem.* **2005**, *15*, 1332–1342.
26. Johnson, N. J. J.; Sangeetha, N. M.; Boyer, J.-C.; van Veggel, F. C. J. M. Facile Ligand-Exchange with Polyvinylpyrrolidone and Subsequent Silica Coating of Hydrophobic Upconverting β-$NaYF_4$:Yb^{3+}/Er^{3+} Nanoparticles. *Nanoscale* **2010**, *2*, 771–777.
27. Tong, S.; Hou, S.; Ren, B.; Zheng, Z.; Bao, G. Self-Assembly of Phospholipid-PEG Coating on Nanoparticles through Dual Solvent Exchange. *Nano Lett.* **2011**, *11*, 3720–3726.
28. Johnson, N. J. J.; Korinek, A.; Dong, C.; van Veggel, F. C. J. M. Self-Focusing by Ostwald Ripening: A Strategy for Layer-by-Layer Epitaxial Growth on Upconverting Nanocrystals. *J. Am. Chem. Soc.* **2012**, *134*, 11068−11071.
29. Lakowicz, J. R. Principles of Fluorescence Spectroscopy. 3rd ed.; Springer Science+Business Media, LLC: 2006.
30. Shannon, R. D. J. Revised Effective Ionic Radii and Systematic Study of Inter Atomic Distances in Halides and Chalcogenides. *Acta Cryst.* **1976**, *A32*, 751–767.
31. Johnson, N. J. J.; van Veggel, F. C. J. M. Lanthanide-Based Heteroepitaxial Core–Shell Nanostructures: Compressive versus Tensile Strain Asymmetry. *ACS Nano* **2014**, *8*, 10517–10527.
32. Abel, K. A.; Boyer, J.-C.; Andrei, C. M.; van Veggel, F. C. J. M. Analysis of the Shell Thickness Distribution on $NaYF_4$/$NaGdF_4$ Core/Shell Nanocrystals by EELS and EDS. *J. Phys. Chem. Lett.* **2011**, *2*, 185–189.
33. Diamente, P. R.; van Veggel, F. C. J. M. Water-Soluble Ln^{3+}-Doped LaF_3 Nanoparticles: Retention of Strong Luminescence and Potential as Biolabels. *J. Fluoresc.* **2005**, *15*, 543−551.
34. Lao, A.; Yu, H.; Jin, J.; Zhang, X.; Guo, Y.; Shi, Y.; Fu, Y.; Gao, S.; Zhao, L. Direct Evidence for Transformation of Multiple Active Crystallographic Sites' Symmetry in β-$NaGdF_4$:Eu^{3+} Nanocrystals. *J. Alloys Comp.* **2016**, *67*, 113–119.
35. Tu, D.; Liu, Y.; Zhu, H.; Li, R.; Liu, L.; Chen, X. Breakdown of Crystallographic Site Symmetry in Lanthanide-Doped $NaYF_4$ Crystals. *Angew. Chem. Int. Ed.* **2013**, *125*, 1166–1171.

36. Stouwdam, J. W.; Hebbink, G. A.; Huskens, J.; van Veggel, F. C. J. M. Lanthanide-Doped Nanoparticles with Excellent Luminescent Properties in Organic Media. *Chem. Mater.* **2003**, *15*, 4604–4616.
37. Garbuzenko, O.; Barenholz, Y.; Priev, A. Effect of Grafted PEG on Liposome Size and on Compressibility and Packing of Lipid Bilayer. *Chem. Phys. Lipids* **2005**, *135*, 117–129.
38. Wong, J. Y.; Kuhl, T. L.; Israelachvili, J. N.; Mullah, N.; Zalipsky, S. Direct Measurement of a Tethered Ligand-Receptor Interaction Potential. *Science* **1997**, *275*, 820–822.
39. Haran, N.; Shporer, M. Study of Water Permeability through Phospholipid Vesicle Membranes by 17-O NMR. *Biochimica et Biophysica Acta* **1976**, *426*, 638–646.
40. Beranová, L.; Humpolíčková, J.; Sýkora, J.; Benda, A.; Cwiklik, L.; Jurkiewicz, P.; Gröbner, G.; Hof, M. Effect of Heavy Water on Phospholipid Membranes: Experimental Confirmation of Molecular Dynamics Simulations. *Phys. Chem. Chem. Phys.* **2012**, *14*, 14516–14522.
41. Tokutake, N.; Jing, B.; Regen, S. L. Probing the Hydration of Lipid Bilayers Using a Solvent Isotope Effect on Phospholipid Mixing. *Langmuir* **2004**, *20*, 8958–8960.
42. Buera, M. d. P.; Levi, G.; Karel, M. Glass Transition in Poly(vinylpyrrolidone): Effect of Molecular Weight and Diluents. *Biotechnol. Prog.* **1992**, *8*, 144–148.
43. Zeng, X.; Zhou, B.; Gao, Y.; Wang, C.; Li, S.; Yeung, C. Y.; We, W. Structural Dependence of Silver Nanowires on Polyvinyl pyrrolidone (PVP) Chain Length. *Nanotechnology* **2014**, *25*, 495601.
44. Bonnet, C. S.; Fries, P. H.; Gadelle, A.; Gambarelli, S.; Delangle, P. A Rigorous Framework To Interpret Water Relaxivity. The Case Study of a Gd(III) Complex with an α-Cyclodextrin Derivative. *J. Am. Chem. Soc.* **2008**, *130*, 10401–10413.
45. Belorizky, E.; Fries, P. H.; Helm, L.; Kowalewski, J.; Kruk, D.; Sharp, R. R.; Westlund, P.-O. Comparison of Different Methods for Calculating the Paramagnetic Relaxation Enhancement of Nuclear Spins as a Function of the Magnetic Field. *J. Chem. Phys.* **2008**, *128*, 052315.
46. Fries, P. H.; Gateau, C.; Mazzanti, M. Practical Route to Relative Diffusion Coefficients and Electronic Relaxation Rates of Paramagnetic Metal Complexes in Solution by Model-Independent Outer-Sphere NMRD. Potentiality for MRI Contrast Agents. *J. Am. Chem. Soc.* **2005**, *127*, 15801–15814.
47. Alvares, R. D. A.; Gautam, A.; Prosser, R. S.; van Veggel, F. C. J. M.; Macdonald, P. M. Shell versus Core Dy^{3+} Contributions to NMR Water Relaxation in Sodium Lanthanide Fluoride Core−Shell Nanoparticles. An Investigation Using O^{-} 17 and H^{-} 1 NMR. *J. Phys. Chem. C* **2017**, *121*, 17552−17558.
48. Kruk, D.; Korpała, A.; Taheri, S. M.; Kozłowski, A.; Förster, S.; Rössler, E. A. ^{1}H Relaxation Enhancement Induced by Nanoparticles in Solutions: Influence of Magnetic Properties and Diffusion. *J. Chem. Phys.* **2014**, *140*, 174504.

TOC Graphic

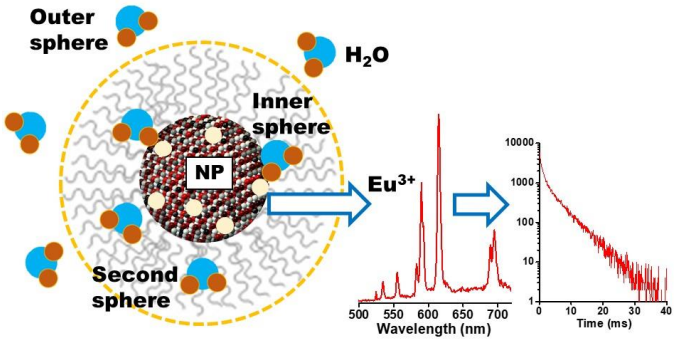
Outer sphere
H_2O
Inner sphere
NP
Second sphere
Eu^{3+}
500 550 600 650 700
Wavelength (nm)
10000
1000
100
10
1
0 10 20 30 40
Time (ms)